2-2017

Superior performance of continuous over pulsatile flow ventricular assist devices in the single ventricle circulation: A computational study

Tyler Schmidt

David Rosenthal

Olaf Reinhartz

Kirk Riemer

Fei He

See next page for additional authors

Authors

Tyler Schmidt, David Rosenthal, Olaf Reinhartz, Kirk Riemer, Fei He, Tain-Yen Hsia, Alison Marsden, and Ethan Kung

Superior performance of continuous over pulsatile flow ventricular assist devices in the single ventricle circulation: A computational study

Tyler Schmidt[1], David Rosenthal[2], Olaf Reinhartz[3], Kirk Riemer[3], Fei He[1], Tain-Yen Hsia[4], Alison Marsden[5], Ethan Kung[1,6] for the Modeling Of Congenital Hearts Alliance (MOCHA)+ Investigators

Citation:
Schmidt T, Rosenthal D, Reinhartz O, Riemer K, He F, Hsia TY, Marsden A, Kung E, MOCHA Investigators. "Superior performance of continuous over pulsatile flow ventricular assist devices in the single ventricle circulation: A computational study." *Journal of Biomechanics*. 52:48-54 (2017)
https://doi.org/10.1016/j.jbiomech.2016.12.003

Corresponding Author:
Ethan Kung
Departments of Mechanical Engineering and Bioengineering
Clemson University, Fluor Daniel Engineering Innovation Building
Clemson, SC 29634
Tel: (650) 307-5557
Fax: (864) 656-4435
E-mail: ekung@clemson.edu

Keywords: ventricular assist device, single ventricle, pediatric, ventricular suction, lumped-parameter network

ABSTRACT

This study compares the physiological responses of systemic-to-pulmonary shunted single ventricle patients to pulsatile and continuous flow ventricular assist devices (VADs). Performance differences between pulsatile and continuous flow VADs have been clinically observed, but the underlying mechanism remains poorly understood. Six systemic-to-pulmonary shunted single ventricle patients (mean BSA=0.30 m^2) were computationally simulated using a lumped-parameter network tuned to match patient specific clinical data. A first set of simulations compared current clinical implementation of VADs in single ventricle patients. A second set modified pulsatile flow VAD settings with the goal to optimize cardiac output (CO). For all patients, the best-case continuous flow VAD CO was at least 0.99 L/min greater than the optimized pulsatile flow VAD CO (p=0.001). The 25 and 50 mL pulsatile flow VADs exhibited incomplete filling at higher heart rates that reduced CO as much as 9.7% and 37.3% below expectations respectively. Optimization of pulsatile flow VAD settings did not achieve statistically significant (p<0.05) improvement to CO. Results corroborate clinical experience that continuous flow VADs produce higher CO and superior ventricular unloading in single ventricle patients. Impaired filling leads to performance degradation of pulsatile flow VADs in the single ventricle circulation.

1. Introduction

Children born with single ventricle congenital heart defects require staged surgical intervention to enable survival. The first of three stages involves insertion of a systemic-to-pulmonary shunt that provides the infant's only source of pulmonary blood flow. However, patients remain at risk of heart failure (HF) due to increased volume loading on the single working ventricle (Gewillig, 2005). A ventricular assist device (VAD) can be used as mechanical bridge support for these patients. VADs have been used in single ventricle circulations (Calvaruso et al., 2007; Cardarelli et al., 2009; Chu et al., 2007) and normal circulations (Adachi and Fraser, 2011; Hetzer et al., 2006b; Stiller et al., 2003), but survival rates for pediatric patients with congenital heart defects remain approximately 25% lower than those without (Morales et al., 2010) and outcomes worsen further in single ventricle cases. Therefore, increased knowledge of mechanisms affecting VAD performance in single ventricle circulations is needed to improve clinical outcomes for these patients.

VADs can be categorized as either pulsatile or continuous flow. Pulsatile flow VADs emulate the heart's distinct phases of diastole and systole. The Berlin Heart EXCOR VAD remains the only such FDA approved device for infants. VAD blood flow is driven via membrane, and valves are located at the inlet and outlet of this "ventricle." Membrane motion is controlled by an air chamber connected to an external air compressor. By contrast, continuous flow VADs use rotors to produce a pressure rise for a particular flow and rotational speed (Moazami et al., 2013). Continuous flow designs generally have better reliability and smaller size while reducing risk of infection, bleeding, trauma, and thrombus (Cheng et al., 2014; Drews et al., 2008; Feller et al., 2007; Kato et al., 2011). While continuous flow devices are now used extensively in adults and older children, none are specifically designed for long-term use in infants. Successful bridge treatment of pediatric patients with continuous flow VADs has been demonstrated (Miera et al., 2011), however further experience is needed in single ventricle circulations. Studies have suggested pulsatile flow VADs may promote better ventricular unloading and more natural physiology (Cheng et al., 2014; Drews et al., 2008; Klotz et al., 2004), however continuous flow VADs may encourage faster recovery of myocardial tissue due to less pulsatile trauma on the heart tissue (Frazier et al., 2004; Frazier and Myers, 1999).

Computational simulations of the cardiovascular system can model the interaction of VADs and other devices with circulatory physiology and predict hemodynamics. Lumped-parameter networks (LPN) and state space models offer a reduced-order modeling approach by making an analogy to electrical circuits and forming a system of ordinary differential equations (ODEs) solved by numerical integration (Ferreira et al., 2005; Kung et al., 2014). In this study, we will use an LPN model to assess VAD performance for our patient cohort. Three dimensional computational fluid dynamics (CFD) methods can obtain greater hemodynamic detail (Migliavacca et al., 2006; Peng et al., 2012), but coupling of VAD CFD simulations to physiologic models has only recently been accomplished (Neidlin et al., 2016). This study improves over the previous work by incorporating a model describing ventricular suction induced by a VAD.

This study aims to understand physiological responses of stage 1 single ventricle patients to pulsatile and continuous flow VADs and to identify mechanistic explanations for differences in performance. This will be evaluated on cohort and patient specific levels. Recommendations for achieving optimal VAD performance in single ventricle patients will be provided within operational limitations of the VADs.

2. Methods

2.1. Overview of Study

The LPN used in this study (Fig. 1) was based on our previous work (Kung et al., 2014). To simulate VAD support, the inflow and outflow cannulas were connected to the ventricle and aorta respectively. In clinical practice, the outflow cannula could be attached to one of several locations near the aorta, such as the neoaorta or innominate artery. In the LPN, which is a simplified representation of vasculature, these locations each correspond to the aortic node. A connection between the aorta and pulmonary arteries represented the systemic-to-pulmonary shunt. Respiration effects were assumed negligible.

Clinical measurements from six stage 1 single ventricle patients (cohort body surface area (BSA) range 0.26-0.34 m^2; mean 0.30 m^2) were obtained from the Great Ormond Street Hospital, Medical University of South Carolina, and University of Michigan. For the LPN simulations to accurately replicate each patient's unique physiology, the LPN element values were tuned using a process similar to our previous works (Corsini et al., 2015, 2014; Kung et al., 2013) to match individual patient's clinical measurements. Once tuning was complete, ventricular contractility was set to zero to simulate HF.

2.2. Simulation Setup and Protocol

We have previously reported a clinical case of extracorporeal implementation of the Revolution VAD (Sorin Group, Italy) in a stage 1 single ventricle patient via 9 mm inner diameter (ID) Berlin Heart cannulas (Lal et al., 2014). However, insufficient data existed to construct a computational model for the Revolution VAD. Therefore, we constructed a HeartWare VAD (HeartWare Inc., Framingham, Massachusetts) model for this study to resemble the continuous flow VAD scenarios similar to our previous clinical experience. Due to the similar continuous flow centrifugal designs of the HeartWare and Revolution VADs, they would produce the same hemodynamics when generating the same pressure head. The only variable setting for the continuous flow VAD was revolutions per minute (RPM).

We modeled the Berlin Heart EXCOR VAD (Berlin Heart GmbH, Berlin, Germany) for the pulsatile flow scenarios in this study. Variable VAD settings for the Berlin Heart were the device size, "heart rate" (HR), peak filling (P_{DIA}) and ejection (P_{SYS}) pressures, and diastolic filling ratio (DFR), which is the time ratio of diastole to the total VAD period.

Two primary sets of simulations were done. The first emulated current clinical implementation of VADs specific to stage 1 single ventricle patients. The pulsatile flow VAD was simulated with the following ranges of settings: HR (15-

105 BPM for 10 and 25 mL, 15-75 BPM for 50 mL), P_{DIA} (-40 mmHg), P_{SYS} (mean aortic pressure+100 mmHg), and DFR (60%). The continuous flow VAD was simulated with rotor speeds from 1800-3400 RPM. Cannula dimensions (Table 1) specified by the manufacturers were used. The second set of simulations investigated changes to pulsatile flow peak pressure and DFR settings to optimize cardiac output.

The system of ODEs describing the LPN were solved with a fourth order Runge-Kutta time-integration method using FORTRAN (IBM Corp., Armonk, New York), and data were analyzed using MATLAB (MathWorks Inc., Natick, Massachusetts). After simulations reached periodicity, data from the last cardiac period were used in the analyses.

2.3. Statistics

To determine statistical significance, hypothesis testing with *p*-values was done assuming a normal distribution. For this study, the null hypothesis was that there is no difference in results between two samples. The threshold for statistical significance was 0.05. The *t*-statistic was used, and the probability for a two-tailed distribution was calculated.

2.4. Ventricular Assist Device Modeling

2.4.1. Pulsatile Flow VAD

The Berlin Heart comes in several sizes ranging from 10 to 80 mL. The 10 and 25 mL sizes are common for pediatric use (Hetzer et al., 2006a; Stiller et al., 2003), and the 50 mL size is also occasionally used to achieve higher CO. Since the Berlin Heart is controlled by the external air compressor, the model prescribed VAD pressure, P_{COMP}, as a sinusoidal function (Fig. A1)

$$P_{COMP} = \begin{cases} P_{SYS}\left(\sin\left(\frac{t*\pi}{(1-DFR)*t_{VAD}}\right)\right)^{0.1} & systole \\ P_{DIA}\sin\left(\frac{(t-(1-DFR)*t_{VAD})*\pi}{DFR*t_{VAD}}\right) & diastole \end{cases} \quad (1)$$

where t_{VAD} is the time of one VAD period and DFR is the diastolic filling ratio (a number between zero and one). The air compressor is limited to HRs up to approximately 110, 100, and 60 BPM for the 10, 25, and 50 mL sizes respectively.

2.4.2. Continuous Flow VAD

For continuous flow VADs, little pulsatility exists once equilibrium occurs between the VAD and the patient's physiology. We used experimental data from literature for the HeartWare VAD to create trendlines (Fig. A2) in the form

$$\Delta P_{VAD} = AQ_{VAD}^2 + BQ_{VAD} + C \quad (2)$$

where ΔP_{VAD} is the pressure rise across the VAD, Q_{VAD} is the flowrate through the VAD, and *A*, *B*, and *C* are constants dependent on the VAD RPM (Moazami et al., 2013).

2.5. Ventricular Suction Caused by VAD Operation

We define resistance due to ventricular collapse induced by a VAD as the ventricular suction resistance, R_{SUC} (mmHg**.**s/mL). If the VAD attempts to draw

blood from the ventricle below its reference volume, which results in a negative ventricular pressure, the ventricle begins to collapse. When this occurs, tissue may be drawn into the cannula or the septum may be drawn closer to the cannula (Salamonsen et al., 2015), both of which can inhibit blood flow. Several models have been proposed in literature (Choi, 1998; Lim et al., 2010; Schima et al., 1990; Yu and Porter, 2006) to describe ventricular suction resistance induced by VADs in various animal experiments.

The ventricular suction models from these previous studies did not produce suction responses during continuous flow VAD simulations consistent with our clinical observations. Therefore, we developed a new model containing two components that improve its realism (Appendix B). We first developed an allometric scaling law relating R_{SUC} to BSA to generalize the model. Second, we combined experimental data from several prior works to create a ventricular suction model (R^2=0.72) suitable for our cohort

$$R_{SUC} = \begin{cases} 0 & P_{SV} > P_{TH} \\ 0.2623(0.9787^{P_{CAN}} - 1)BSA^{-0.3492} & P_{SV} \leq P_{TH} \end{cases} \quad (3)$$

where P_{CAN} is the inflow cannula pressure, P_{SV} is the ventricular pressure, and P_{TH} is the threshold pressure set to 0 mmHg. If complete flow obstruction (when the inflow cannula attaches to the collapsed ventricular wall) occurs, the value of P_{TH} is set to the positive ventricular pressure needed to overcome the negative cannula pressure and "pop off" the cannula from the wall. In this scenario P_{TH} is calculated as

$$P_{TH} = \frac{|P_{CAN}(D_{CAN})^2|}{8031BSA} \quad (4)$$

where D_{CAN} is the inflow cannula ID in mm. After complete flow obstruction ends, P_{TH} is reset to 0 mmHg. The complete developments of equations 3 and 4 are described in Appendix B.

2.6. Passive Ventricular Pressure-Volume Relationship During Suction

To properly utilize equation 3, we require a passive ventricular pressure-volume relationship to replicate a physiologically appropriate trend at negative pressures. This has been investigated by several studies (Burkhoff et al., 2005; Gilbert and Glantz, 1989; Nikolić et al., 1988). We adopted the results of Nikolić et al. since they presented sufficient supporting data to reconstruct a usable model

$$P_{SV} = S_n \ln\left(\frac{V_{SV}}{V_0}\right) \quad (5)$$

where S_n is a stiffness property, V_{SV} is the ventricular volume, and V_0 is the reference volume for which pressure is zero. S_n was independent of body mass, therefore the mean value from the study was used.

3. Results

3.1. LPN Tuning

All pre-HF simulation results (Table C2) matched clinical measurements within ±10% except for atrial pressure (up to ±30.6%) in three patients, pulmonary flow (up to ±19.8%) in two patients, and pulmonary pressure (±11.6%) in one patient. However, clinical measurements of pulmonary flow were subject

to fluctuations from turbulence in some patients, therefore we felt confident that convergence of other parameters to clinical measurements was sufficient to demonstrate the LPN represented patient physiologies well.

3.2. Simulation of VAD Implementation in Clinical Practice

3.2.1. Pulsatile Flow VAD

For a pulsatile flow VAD, the expected cardiac output (CO) is the VAD volume times VAD HR when flow through the aortic valve is zero. At very low HRs for the 10 and 25 mL sizes, additional flow through the aortic valve produced by atrial contraction resulted in CO greater than the expected CO; these scenarios would not be observed in reality since such low HR settings would not be used clinically. Expected CO was achieved for the 10 mL Berlin Heart at all HRs (Fig. 2). However, reductions from expected CO occurred at higher HRs for the 25 and 50 mL sizes (Figs. 2 and 3a).

Decreases in CO from expected with the 25 and 50 mL sizes were examined more closely by investigating the VAD's filling and ejection performance. For a pulsatile flow VAD to attain the expected CO, it must both fill and eject blood completely in each cardiac period. Stroke volumes (SV) of the 25 and 50 mL size VAD both showed decreases from expected at higher HRs (Fig. 4). V_{MIN} was 0 mL for all VAD sizes at all HRs, which implied that incomplete ejection never occurred. Therefore, the drops in SV were solely due to incomplete filling. We investigated several approaches to modifying VAD settings in order to reduce incomplete filling and optimize CO, however, no statistically significant improvement in CO was achieved (Appendix E).

3.2.2. Continuous Flow VAD

For the continuous flow VAD, RPM was the only variable setting. CO of the HeartWare VAD increased steadily with RPM until reaching a maximum of 3.10 L/min at 3000 RPM (Fig. 3b). Beyond 3000 RPM, temporary periods of complete flow obstruction occurred and resulted in alternating periods of flow and no flow. This increased R_{SUC} and decreased CO. Ventricular and atrial pressures both decreased steadily as unloading improved until reaching minimums of -2.83 and -0.47 mmHg at 3000 RPM. The reduction in P_{SA} occurred due to propagation of volume unloading upstream from the ventricle and demonstrated the VAD's ability to alleviate congestion. We also note the phasic suction response (Fig. 5) occurring in simulations of three patients at high RPMs with the continuous flow VAD. In those patients, P_{CAN} approached negative pressures low enough (e.g. -200 mmHg) to result in complete flow obstruction where the ventricular wall was sucked onto the opening of the inflow cannula.

3.3. Patient Specific Results

Patient specific results were investigated to identify patient specific factors affecting outcomes and the differences between pulsatile and continuous flow VAD support at an individual level (Table 2). Detailed physiological results of these simulations are in Table D2.

Due to volume loading from the pulmonary shunt, significant CO is desired in order to produce favorable clinical outcomes. The target CO for these pediatric patients is $BSA*CI_{target}$, where CI_{target} is 6 L/min/m^2. The target CO was attained for all patients with both pulsatile and continuous flow. For all six patients, the continuous flow VAD CO was at least 0.99 L/min greater than the optimized pulsatile flow VAD CO. Optimizing the settings of the pulsatile flow VAD increased CO for four patients, but the largest individual increase was only 0.07 L/min (3.0%). Therefore, the current clinical protocol for pulsatile flow VAD settings is close to optimum as-is.

Pre-HF CO was the best predictor of VAD supported CO for both VAD types. This was true for each patient in the cohort except for patient E. Patient E had an atrial reference volume of 14.1 mL compared to a mean of 1.4 mL for the other five patients. This reduced the VAD CO for patient E because patient E required a larger atrial volume than those of other patients to maintain the same atrial pressure needed to drive ventricular filling.

For pulsatile flow, the 25 mL size produced greater CO than the 50 mL size in three patients. Two of these patients (A and C) possessed the lowest pre-HF CO and the other was patient E, who possessed the larger atrial reference volume. Since the 25 mL size requires half as much filling per VAD period compared to the 50 mL size, the likelihood of incomplete filling is reduced. This suggests using a smaller size pulsatile flow VAD for patients with low pre-HF CO.

Phasic complete flow obstruction occurred in simulations of three patients with the HeartWare VAD. These patients had three of the four lowest pre-HF CO. This indicates that optimal outcomes for patients with low pre-HF CO will occur at lower VAD RPM settings.

4. Discussion

It is dominantly observed in anecdotal clinical experiences of VAD support in single ventricle patients that continuous flow results in superior outcomes. However, these clinical experiences are rare and have not been well documented or published. This computational study provides crucial data as an important first step to understand the physiological impacts of continuous versus pulsatile flow VAD support to the single ventricle circulation and to illustrate the potential underlying mechanisms leading to these impacts. Since stage 1 patients have parallel systemic and pulmonary circulations, greater CO is needed. Therefore, these results should not be generalized to Fontan or double ventricle patients.

Following clinical protocol, the maximum cohort mean CO were 2.23 and 3.10 L/min with the Berlin Heart and HeartWare VAD respectively. The mean atrial and ventricular pressures decreased to P_{SA}=1.90 mmHg and P_{SV}=0.29 mmHg (Berlin Heart) and P_{SA}=-0.47 mmHg and P_{SV}=-2.83 mmHg (HeartWare VAD) from unsupported heart failure pressures (Table D1). These results demonstrated that, while congestion was alleviated with both pulsatile and continuous flow VAD support, the continuous flow VAD produced superior maximum CO (p=0.001). These findings corroborate current clinical experience of VAD implementation in single ventricle patients.

Reduction of SV at higher HRs for the pulsatile flow VAD occurred due to incomplete filling. For the 50 mL size from 45 to 75 BPM, V_{MAX} decreased from 47.5 to 33.2 mL despite fairly constant R_{SUC}. This implied incomplete filling resulted from a combination of ventricular suction and reduced VAD diastolic time as HR increased.

The concept of duty cycle can explain why continuous flow produced superior CO. The continuous flow VAD effectively has a 100% duty cycle since filling and ejection are synonymous. The pulsatile flow VAD has a reduced duty cycle since it can only fill or eject at any given time. Other challenges to attaining expected CO for pulsatile flow in clinical practice can also be identified. For the 25 and 50 mL Berlin Heart, incomplete filling presented at higher HRs because time for filling was reduced. Producing a high CO with a pulsatile flow VAD necessitates using a high HR, which then results in incomplete filling. Despite optimizing VAD peak pressure and DFR settings, the VAD's increased demand for blood during filling only tended to increase suction resistance rather than CO. Incomplete ejection is another potential limiting factor to CO. However, since ejection occurs separately from filling, P_{SYS} can be increased to eliminate incomplete ejection with no adverse effect on filling performance. This was successfully demonstrated during the simulations of modified pulsatile flow VAD settings when P_{SYS} was increased by 100 mmHg from clinical recommendation to prevent incomplete ejection (case 5, Table E1). Therefore, incomplete ejection should generally not be a limiting factor of CO for a pulsatile flow VAD.

In several patients, simulating the continuous flow VAD at high RPMs produced a phasic flow obstruction response. During the obstruction, no flow exited from the ventricle to the VAD or aorta, and ventricular pressure increased as blood returned from the atrium until a pressure sufficient to "pop off" the cannula was reached and flow resumed. This resulted in the alternating behavior between flow and complete flow obstruction (Fig. 5).

4.1. Limitations and Future Work

Since there is a lack of ventricular suction data specific to pediatric, single ventricle patients, equation 3 will require experimental validation in future studies. Despite this, results from suction model simulation testing (Table B1) provided confidence the model we developed improved over existing models at producing physiologically realistic results. Additionally, the new model accounted for the possibility of complete flow obstruction, which prior models did not. Even though equation 3 was developed from an amalgam of data applicable to various anatomies, it is strongly recommended that future computational studies employ a similar validation process as described in Appendix B.

There remains a need for improvement to models describing ventricular suction resistance and the passive pressure-volume relationship at negative ventricular pressures. The majority of existing work has focused on animal experiments, and it remains unknown how well these translate to humans. It could be beneficial to explore *in-vivo* experiments and human data. This would provide much needed advancements to critical components of simulations involving VADs. While *in-vitro* experiments with *postmortem* hearts could be

orchestrated more easily, the lack of muscle tone and tissue would not be representative of a clinical situation. Additionally, it would be beneficial for future computational studies to incorporate cardiovascular feedback mechanisms to simulate a patient's long-term response to VAD treatment.

Since ventricular contractility may be partially present during HF, synchronization of the VAD to the patient's native heart can impact the efficacy of filling and ejection and consequently CO. Simulations of co- and counter-pulsation methods for pulsatile and pseudo-pulsatile continuous flow VADs show small physiological differences among syncing schemes (Neidlin et al., 2016; Shi et al., 2007), but incorporating our improved suction model may alter these previous findings.

4.2. Conclusion

In summary, our results predict VAD treatment outcomes for stage 1 single ventricle patients by comparing performance between the pulsatile flow Berlin Heart EXCOR VAD and continuous flow HeartWare VAD. We first developed an improved model for ventricular suction resistance using data from prior literature. We then showed the continuous flow VAD produced greater CO by at least 0.99 L/min (p=0.001) for all patients. The CO produced by the 50 mL Berlin Heart was as much as 1.4 L/min (37.3%) below expected due to incomplete filling caused by ventricular suction and shorter diastolic time at high HRs. Optimizing VAD peak pressure and DFR settings from clinical recommendations increased CO by at most 0.07 L/min for each patient and failed to produce a statistically significant (p<0.05) improvement. The Berlin Heart's ability to produce CO ultimately remained filling limited. Further work is needed to validate these findings over a broader population. This study elucidates underlying mechanisms affecting outcomes of pulsatile and continuous flow VAD support in single ventricle patients and quantifies the impacts of ventricular suction, ventricular collapse, and incomplete filling on VAD supported physiologies.

Conflict of Interest Statement

There are no conflicts of interest associated with this work.

Acknowledgments

This work was supported by the Leducq Foundation as part of the Transatlantic Network of Excellence for Cardiovascular Research, an American Heart Association Postdoctoral Fellowship (12POST11250009), a Burroughs Wellcome Fund Career Award at the Scientific Interface, and the Department of Mechanical Engineering at Clemson University.

Reference

Adachi, I., Fraser, C.D., 2011. Mechanical circulatory support for infants and small children. Semin. Thorac. Cardiovasc. Surg. Pediatr. Card. Surg. Annu. 14, 38–44. doi:10.1053/j.pcsu.2011.01.008

Bergman, T.L., Lavine, A.S., Incropera, F.P., DeWitt, D.P., 2011. Introduction to

Heat Transfer, 6th ed. John Wiley & Sons, Inc, Jefferson City, MO.

Burkhoff, D., Mirsky, I., Suga, H., 2005. Assessment of systolic and diastolic ventricular properties via pressure-volume analysis: a guide for clinical, translational, and basic researchers. Am J Physiol Hear. Circ Physiol 289, H501–H512. doi:10.1152/ajpheart.00138.2005

Calvaruso, D.F., Ocello, S., Salviato, N., Guardì, D., Petruccelli, D.F., Rubino, A., Fattouch, K., Cipriani, A., Marcelletti, C.F., 2007. Implantation of a berlin heart as single ventricle by-pass on fontan circulation in univentricular heart failure. ASAIO J. 53, e1-2. doi:10.1097/MAT.0b013e31815a2500

Cardarelli, M.G., Salim, M., Love, J., Simone, S., Tumulty, J., Conway, D., Griffith, B., 2009. Berlin heart as a bridge to recovery for a failing fontan. Ann. Thorac. Surg. 87, 943–946. doi:10.1016/j.athoracsur.2008.07.086

Cheng, A., Williamitis, C.A., Slaughter, M.S., 2014. Comparison of continuous-flow and pulsatile-flow left ventricular assist devices: is there an advantage to pulsatility? Ann. Cardiothorac. Surg. 3, 573–81. doi:10.3978/j.issn.2225-319X.2014.08.24

Choi, S., 1998. Modeling and Control of Left Ventricular Assist System. University of Pittsburgh.

Chu, M.W.A., Sharma, K., Tchervenkov, C.I., Jutras, L.F., Lavoie, J., Shemie, S.D., Laliberte, E., Calaritis, C., Cecere, R., 2007. Berlin heart ventricular assist device in a child with hypoplastic left heart syndrome. Ann. Thorac. Surg. 83, 1179–81. doi:10.1016/j.athoracsur.2006.08.020

Corsini, C., Baker, C., Baretta, A., Biglino, G., Hlavacek, A.M., Hsia, T.-Y., Kung, E., Marsden, A., Migliavacca, F., Vignon-Clementel, I., Pennati, G., 2015. Integration of Clinical Data Collected at Different Times for Virtual Surgery in Single Ventricle Patients : A Case Study. Ann. Biomed. Eng. 43, 1310–1320. doi:10.1007/s10439-014-1113-6

Corsini, C., Baker, C., Kung, E., Schievano, S., Arbia, G., Baretta, A., Biglino, G., Migliavacca, F., Dubini, G., Pennati, G., Marsden, A., Vignon-Clementel, I., Taylor, A., Hsia, T.-Y., Dorfman, A., 2014. An integrated approach to patient-specific predictive modeling for single ventricle heart palliation. Comput. Methods Biomech. Biomed. Engin. doi:10.1080/10255842.2012.758254

Dawson, T., 2014. Allometric relations and scaling laws for the cardiovascular system of mammals. Systems 2, 168–185. doi:10.3390/systems2020168

Drews, T., Jurmann, M., Michael, D., Miralem, P., Weng, Y., Hetzer, R., 2008. Differences in pulsatile and non-pulsatile mechanical circulatory support in long-term use. J. Hear. Lung Transplant. 27, 1096–1101. doi:10.1016/j.healun.2008.07.007

Feller, E.D., Sorensen, E.N., Haddad, M., Pierson, R.N., Johnson, F.L., Brown, J.M., Griffith, B.P., 2007. Clinical outcomes are similar in pulsatile and nonpulsatile left ventricular assist device recipients. Ann. Thorac. Surg. 83,

1082–1088. doi:10.1016/j.athoracsur.2006.10.034

Ferreira, A., Chen, S., Simaan, M.A., Boston, J.R., Antaki, J.F., 2005. A nonlinear state-space model of a combined cardiovascular system and a rotary pump. Proc. 44th IEEE Conf. Decis. Control. Eur. Control Conf. CDC-ECC '05 2005, 897–902. doi:10.1109/CDC.2005.1582271

Frazier, O.H., Myers, T.J., 1999. Left ventricular assist system as a bridge to myocardial recovery. Ann. Thorac. Surg. 68, 734–741. doi:10.1016/S0003-4975(99)00801-2

Frazier, O.H., Myers, T.J., Westaby, S., Gregoric, I.D., 2004. Clinical experience with an implantable, intracardiac, continuous flow circulatory support device: physiologic implications and their relationship to patient selection. Ann. Thorac. Surg. 77, 133–142. doi:10.1016/S0003-4975(03)01321-3

Gewillig, M., 2005. The fontan circulation. Heart 91, 839–846. doi:10.1136/hrt.2004.051789

Gilbert, J.C., Glantz, S.A., 1989. Determinants of left ventricular filling and of the diastolic pressure-volume relation. Circ. Res. 64, 827–852. doi:10.1161/01.RES.64.5.827

Hetzer, R., Alexi-Meskishvili, V., Weng, Y., Hübler, M., Potapov, E., Drews, T., Hennig, E., Kaufmann, F., Stiller, B., 2006a. Mechanical cardiac support in the young with the berlin heart EXCOR pulsatile ventricular assist device: 15 years' experience. Pediatr. Card. Surg. Annu. 9, 99–108. doi:10.1053/j.pcsu.2006.02.012

Hetzer, R., Potapov, E. V., Stiller, B., Weng, Y., Hubler, M., Lemmer, J., Alexi-Meskishvili, V., Redlin, M., Merkle, F., Kaufmann, F., Hennig, E., 2006b. Improvement in survival after mechanical circulatory support with pneumatic pulsatile ventricular assist devices in pediatric patients. Ann. Thorac. Surg. 82, 917–925. doi:10.1016/j.athoracsur.2006.03.065

Kato, T.S., Chokshi, A., Singh, P., Khawaja, T., Cheema, F., Akashi, H., Shahzad, K., Iwata, S., Homma, S., Takayama, H., Naka, Y., Jorde, U., Farr, M., Mancini, D.M., Christian Schulze, P., 2011. Effects of continuous-flow versus pulsatile-flow left ventricular assist devices on myocardial unloading and remodeling. Circ. Hear. Fail. 4, 546–553. doi:10.1161/CIRCHEARTFAILURE.111.962142

Klotz, S., Deng, M.C., Stypmann, J., Roetker, J., Wilhelm, M.J., Hammel, D., Scheld, H.H., Schmid, C., 2004. Left ventricular pressure and volume unloading during pulsatile versus nonpulsatile left ventricular assist device support. Ann. Thorac. Surg. 77, 143–150. doi:10.1016/S0003-4975(03)01336-5

Kung, E., Baretta, A., Baker, C., Arbia, G., Biglino, G., Corsini, C., Schievano, S., Vignon-Clementel, I.E., Dubini, G., Pennati, G., Taylor, A., Dorfman, A., Hlavacek, A.M., Marsden, A.L., Hsia, T.Y., Migliavacca, F., 2013. Predictive

499 modeling of the virtual Hemi-Fontan operation for second stage single
500 ventricle palliation: Two patient-specific cases. J. Biomech. 46, 423–429.
501 doi:10.1016/j.jbiomech.2012.10.023

502 Kung, E., Pennati, G., Migliavacca, F., Hsia, T.-Y., Figliola, R., Marsden, A.,
503 Giardini, A., 2014. A simulation protocol for exercise physiology in fontan
504 patients using a closed loop lumped-parameter model. J. Biomech. Eng.
505 136, 1–13. doi:10.1115/1.4027271

506 Lal, A.K., Chen, S., Maeda, K., McCammond, A., Rosenthal, D.N., Reinhartz, O.,
507 Yeh, J., 2014. Successful bridge to transplant with a continuous flow
508 ventricular assist device in a single ventricle patient with an aortopulmonary
509 shunt. ASAIO J. 60, 119–121. doi:10.1097/MAT.0000000000000007

510 Lim, E., Dokos, S., Cloherty, S.L., Salamonsen, R.F., Mason, D.G., Reizes, J.A.,
511 Lovell, N.H., 2010. Parameter-optimized model of cardiovascular rotary
512 blood pump interactions. IEEE Trans. Biomed. Eng. 57, 254–266.
513 doi:10.1109/TBME.2009.2031629

514 Miera, O., Potapov, E. V., Redlin, M., Stepanenko, A., Berger, F., Hetzer, R.,
515 Hbler, M., 2011. First experiences with the HeartWare ventricular assist
516 system in children. Ann. Thorac. Surg. 91, 1256–1260.
517 doi:10.1016/j.athoracsur.2010.12.013

518 Migliavacca, F., Balossino, R., Pennati, G., Dubini, G., Hsia, T.-Y., De Leval,
519 M.R., Bove, E.L., 2006. Multiscale modelling in biofluidynamics: application
520 to reconstructive pediatric cardiac surgery. J. Biomech. 39, 1010–1020.
521 doi:10.1016/j.jbiomech.2005.02.021

522 Migliavacca, F., Dubini, G., Pennati, G., Pietrabissa, R., Fumero, R., Hsia, T.Y.,
523 de Leval, M.R., 2000. Computational model of the fluid dynamics in
524 systemic-to-pulmonary shunts. J. Biomech. 33, 549–57. doi:10.1016/s0021-
525 9290(99)00219-5

526 Moazami, N., Fukamachi, K., Kobayashi, M., Smedira, N.G., Hoercher, K.J.,
527 Massiello, A., Lee, S., Horvath, D.J., Starling, R.C., 2013. Axial and
528 centrifugal continuous-flow rotary pumps: a translation from pump
529 mechanics to clinical practice. J. Hear. Lung Transplant. 32, 1–11.
530 doi:10.1016/j.healun.2012.10.001

531 Morales, D.L.S., Zafar, F., Rossano, J.W., Salazar, J.D., Jefferies, J.L., Graves,
532 D.E., Heinle, J.S., Fraser, C.D., 2010. Use of ventricular assist devices in
533 children across the united states: analysis of 7.5 million pediatric
534 hospitalizations. Ann. Thorac. Surg. 90, 1313–1318.
535 doi:10.1016/j.athoracsur.2010.04.107

536 Neidlin, M., Corsini, C., Sonntag, S.J., Schulte-eistrup, S., Schmitz-rode, T.,
537 Steinseifer, U., Pennati, G., Kaufmann, T.A.S., 2016. Hemodynamic analysis
538 of outflow grafting positions of a ventricular assist device using closed-loop
539 multiscale CFD simulations: Preliminary results. J. Biomech. 49, 2718–2725.
540 doi:10.1016/j.jbiomech.2016.06.003

Nikolić, S., Yellin, E.L., Tamura, K., Vetter, H., Tamura, T., Meisner, J.S., Frater, R.W., 1988. Passive properties of canine left ventricle: diastolic stiffness and restoring forces. Circ. Res. 62, 1210–1222. doi:10.1161/01.RES.62.6.1210

Ochsner, G., Amacher, R., Daners, M.S., 2013. Emulation of ventricular suction in a hybrid mock circulation. 2013 Eur. Control Conf. 3108–3112.

Peng, Y., Wu, Y., Tang, X., Liu, W., Chen, D., Gao, T., Xu, Y., Zeng, Y., 2012. Numerical simulation and comparative analysis of flow field in axial blood pumps. Comput. Methods Biomech. Biomed. Engin. 17, 1–5. doi:10.1080/10255842.2012.715156

Salamonsen, R.F., Lim, E., Moloney, J., Lovell, N.H., Rosenfeldt, F.L., 2015. Anatomy and physiology of left ventricular suction induced by rotary blood pumps. Artif. Organs 39, 681–690. doi:10.1111/aor.12550

Schima, H., Honigschnabel, J., Trubel, W., Thoma, H., 1990. Computer simulation of the circulatory system during support with a rotary blood pump. ASAIO J. 36, M252–M254.

Shi, Y., Korakianitis, T., Bowles, C., 2007. Numerical simulation of cardiovascular dynamics with different types of VAD assistance. J. Biomech. 40, 2919–2933. doi:10.1016/j.jbiomech.2007.02.023

Stiller, B., Hetzer, R., Weng, Y., Hummel, M., Hennig, E., Nagdyman, N., Ewert, P., Lehmkuhl, H., Lange, P.E., 2003. Heart transplantation in children after mechanical circulatory support with pulsatile pneumatic assist device. J. Hear. Lung Transplant. 22, 1201–8. doi:10.1016/S1053-2498(02)01233-0

Troy, B.L., Pombo, J., Rackley, C.E., 1972. Measurement of left ventricular wall thickness and mass by echocardiography. Circulation 45, 602–611. doi:10.1161/01.CIR.45.3.602

Yu, Y.-C., Porter, J., 2006. Mathematical modeling of ventricular suction induced by a rotary ventricular assist device. Am. Control Conf. 2006 707–712. doi:10.1109/ACC.2006.1655439

Table and Figure Captions

Fig. 1. Lumped-parameter network for a stage 1 single ventricle circulation on VAD support. $P_{SUBSCRIPT}$, pressure; $Q_{SUBSCRIPT}$, volumetric flowrate; $L_{SUBSCRIPT}$, inductance; $C_{SUBSCRIPT}$, capacitance; $R_{SUBSCRIPT}$, linear resistance; $K_{SUBSCRIPT}$, quadratic resistance; $E_{SUBSCRIPT}$, elastance.

Table 1. Cannula parameters for the Berlin Heart and HeartWare VAD simulations. Values given are from manufacturer specifications when available. * Cannula dimensions simulated for HeartWare VAD were based on Revolution VAD case study (Lal et al., 2014) that used Berlin Heart cannulas. A dash indicates the value was not provided or not applicable (i.e. head ID is same as body ID). ID, inner diameter.

Fig. 2. Expected (VAD stroke volume * VAD heart rate) versus simulated cardiac output of 10 and 25 mL Berlin Heart. Data points represent cohort mean values.

Fig. 3. Resulting physiologies for the (a) 50 mL Berlin Heart and (b) HeartWare VAD. Data points represent cohort mean values. CO, cardiac output; R_{SUC}, suction resistance; P_{SA}, atrial pressure; P_{SV}, ventricular pressure.

Fig. 4. Mean stroke volume (SV) and suction resistance (R_{SUC}) versus VAD heart rate for the 25 and 50 mL Berlin Heart using clinical recommended VAD settings. Data points represent cohort mean values.

Table 2. Patient specific results for pulsatile and continuous flow VADs. CO are mean values for the last cardiac period and are in units of L/min. NI, “no improvement” from clinical recommended VAD settings. P_{DIA}, peak filling pressure; P_{SYS}, peak ejection pressure; P_{AO}, aortic pressure DFR, diastolic filling ratio.

Fig. 5. Demonstration of phasic complete flow obstruction in one patient during continuous flow VAD support. VAD flow (Q_{VAD}) dropped to zero when the cannula pressure (P_{CAN}) decreased rapidly, which represented the start of a complete flow obstruction event. During complete flow obstruction, ventricular volume (not shown) steadily increased with flow from the atrium to the ventricle (Q_{AV}). Ventricular pressure (P_{SV}) was slower to increase since ventricular volume started close to zero in the “flat” region of the passive pressure-volume curve.

Tables

Table 1.

VAD	Inflow Cannula				Outflow Cannula			
	Head ID (mm)	Head Length (mm)	Body ID (mm)	Body Length (mm)	Head ID (mm)	Head Length (mm)	Body ID (mm)	Body Length (mm)
10 mL Berlin Heart	6	18	6	232	6	-	6	250
25 mL Berlin Heart	9	28	12	242	12	-	12	280
50 mL Berlin Heart	9	28	12	242	12	-	12	280
HeartWare VAD*	9	28	12	242	12	-	12	280

Table 2.

Patient	A	B	C	D	E	F
Pre-HF CO	1.29	1.55	1.42	1.60	1.87	1.75
Target VAD CO	1.80	1.56	2.04	1.68	2.04	1.62
Pulsatile Flow						
Control CO	1.92	2.30	2.14	2.24	2.21	2.79
Control Settings	25 mL 90 BPM	50 mL 60 BPM	25 mL 90 BPM	50 mL 45 BPM	25 mL 90 BPM	50 mL 60 BPM
Optimized CO	1.94	2.37	NI	2.26	NI	2.86
Optimized Settings	25 mL 90 BPM 80% DFR	50 mL 60 BPM P_{SYS} = 200+P_{AO} mmHg P_{DIA} = -100 mmHg 80% DFR	NI	50 mL 60 BPM P_{SYS} = 200+P_{AO} mmHg P_{DIA} = -100 mmHg 80% DFR	NI	50 mL 60 BPM P_{SYS} = 200+P_{AO} mmHg P_{DIA} = -100 mmHg 80% DFR
Continuous Flow						
Control CO	3.11	3.36	3.35	3.50	3.31	4.08
Rotor RPM	3400	3200	3000	3200	3400	3400

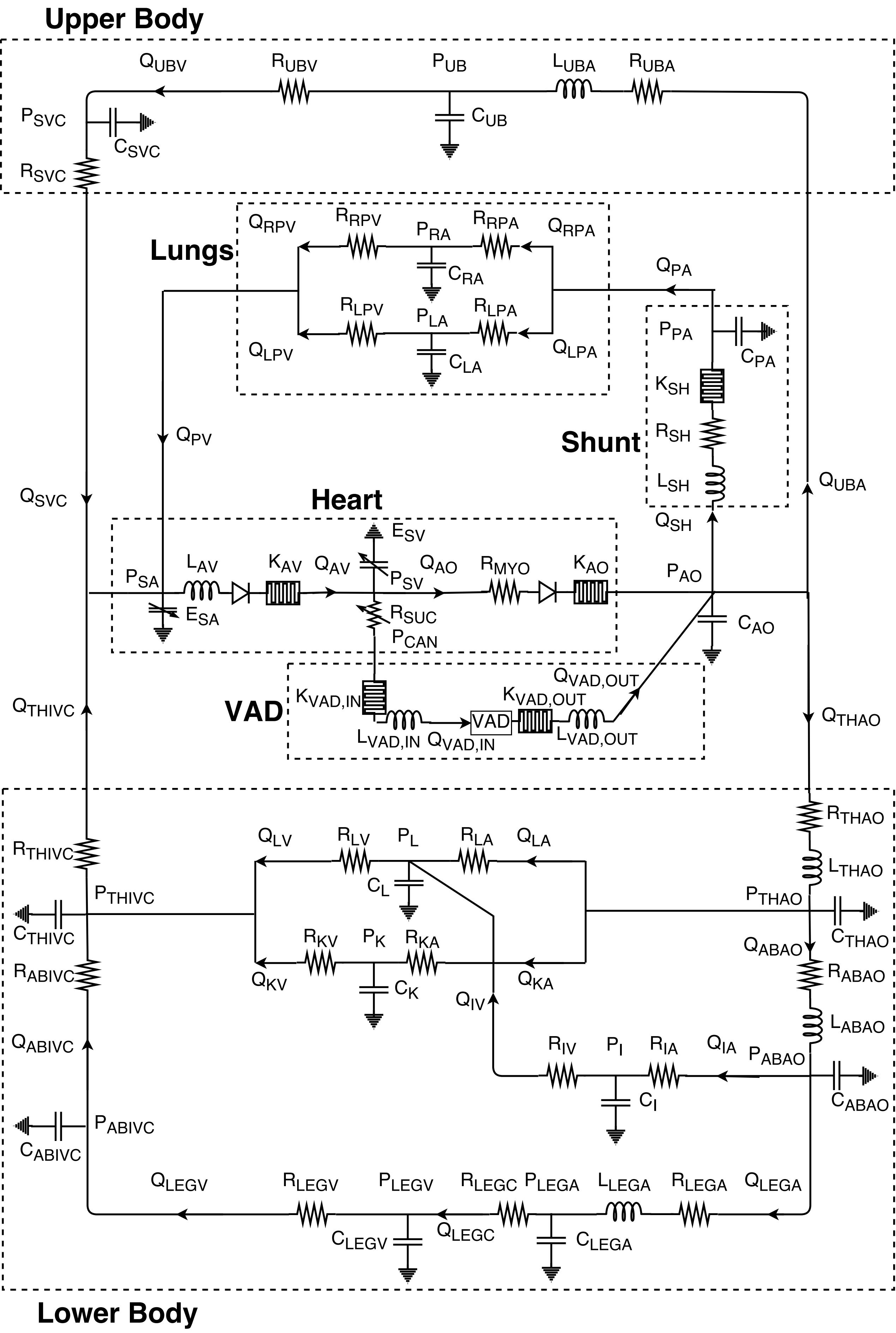
Upper Body
Q_{UBV}
R_{UBV}
P_{UB}
L_{UBA}
R_{UBA}
P_{SVC}
C_{SVC}
C_{UB}
R_{SVC}
Lungs
Q_{RPV}
R_{RPV}
P_{RA}
R_{RPA}
Q_{RPA}
C_{RA}
Q_{PA}
R_{LPV}
P_{LA}
R_{LPA}
Q_{LPV}
C_{LA}
Q_{LPA}
P_{PA}
C_{PA}
K_{SH}
Q_{PV}
Shunt
R_{SH}
L_{SH}
Q_{UBA}
Q_{SVC}
Heart
Q_{SH}
E_{SV}
L_{AV}
K_{AV}
Q_{AV}
Q_{AO}
R_{MYO}
K_{AO}
P_{AO}
P_{SA}
P_{SV}
E_{SA}
R_{SUC}
C_{AO}
P_{CAN}
$K_{VAD,IN}$
$Q_{VAD,OUT}$
$K_{VAD,OUT}$
VAD
Q_{THIVC}
$L_{VAD,IN}$
$Q_{VAD,IN}$
$L_{VAD,OUT}$
Q_{THAO}
R_{THAO}
Q_{LV}
R_{LV}
P_L
R_{LA}
Q_{LA}
L_{THAO}
R_{THIVC}
C_L
P_{THAO}
P_{THIVC}
C_{THIVC}
R_{KV}
P_K
R_{KA}
C_{THAO}
Q_{ABAO}
R_{ABIVC}
Q_{KV}
C_K
Q_{KA}
R_{ABAO}
Q_{IV}
L_{ABAO}
Q_{ABIVC}
R_{IV}
P_I
R_{IA}
Q_{IA}
P_{ABAO}
C_I
C_{ABAO}
P_{ABIVC}
C_{ABIVC}
Q_{LEGV}
R_{LEGV}
P_{LEGV}
R_{LEGC}
P_{LEGA}
L_{LEGA}
R_{LEGA}
Q_{LEGA}
Q_{LEGC}
C_{LEGV}
C_{LEGA}
Lower Body

Fig. 2

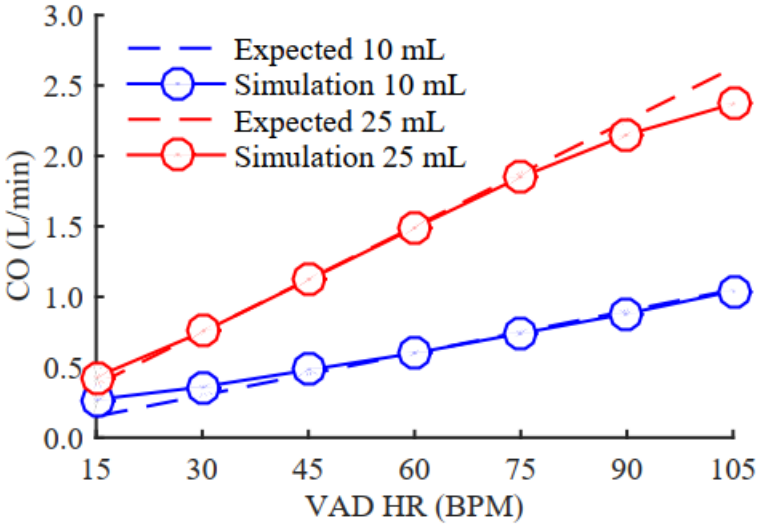
Expected 10 mL
Simulation 10 mL
Expected 25 mL
Simulation 25 mL
CO (L/min)
VAD HR (BPM)

Fig. 3

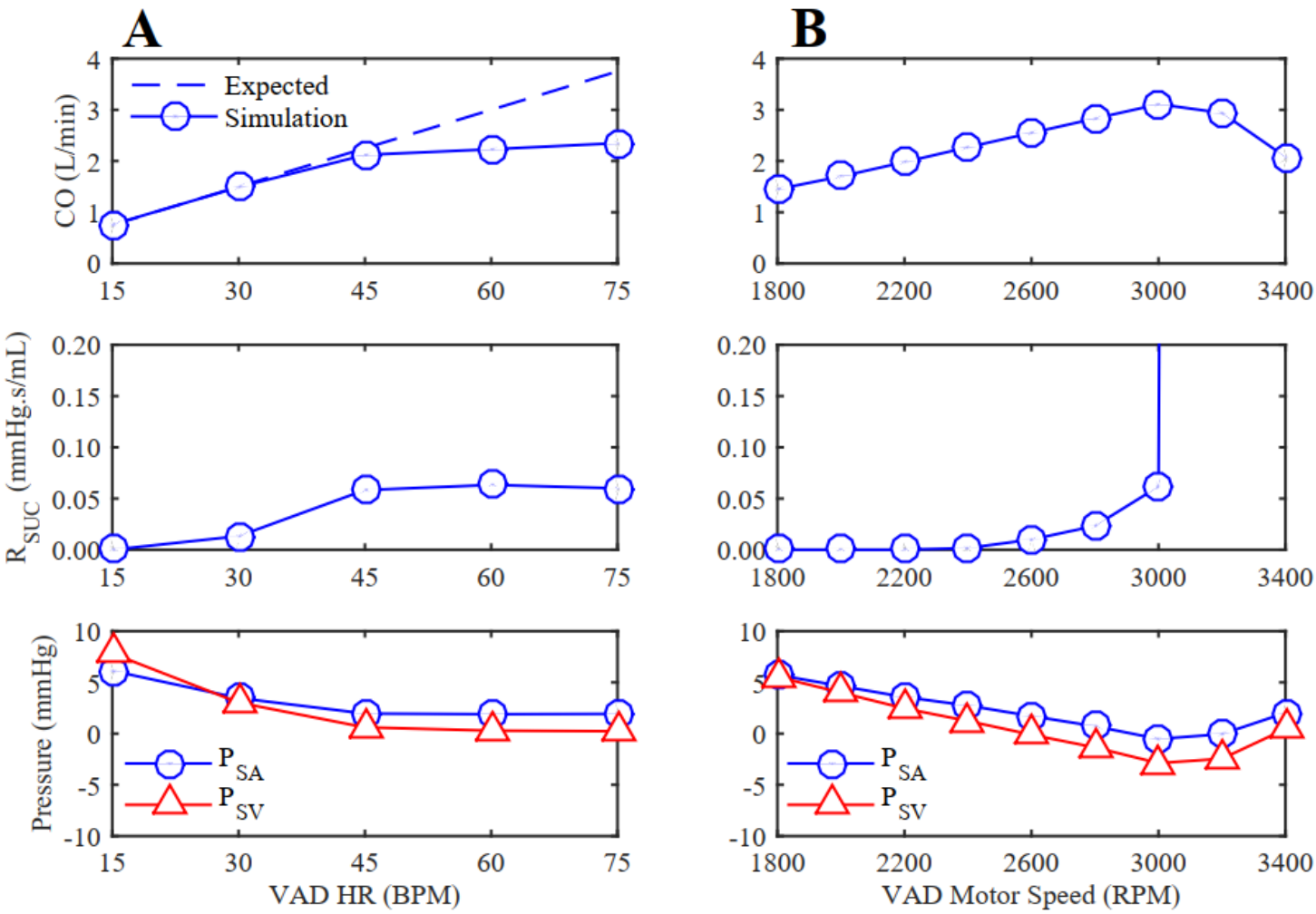
A
B
Expected
Simulation
CO (L/min)
R_{SUC} (mmHg.s/mL)
Pressure (mmHg)
P_{SA}
P_{SV}
VAD HR (BPM)
VAD Motor Speed (RPM)

Fig. 4

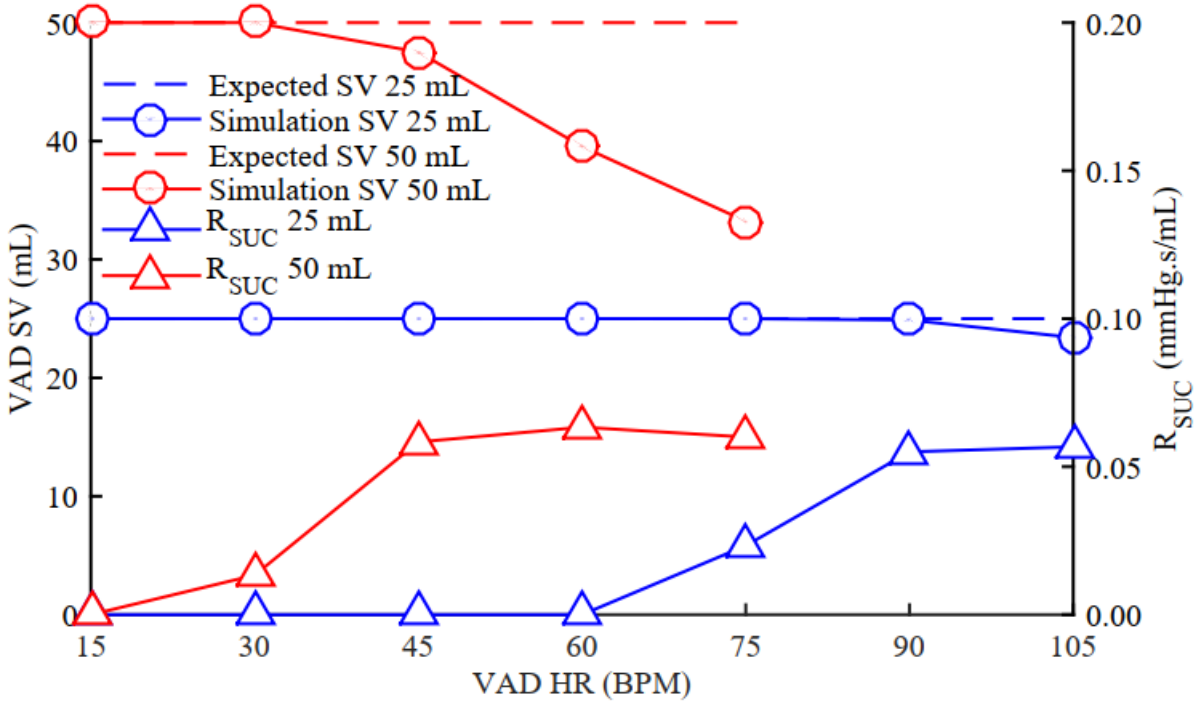
Expected SV 25 mL
Simulation SV 25 mL
Expected SV 50 mL
Simulation SV 50 mL
R_SUC 25 mL
R_SUC 50 mL
VAD SV (mL)
R_SUC (mmHg.s/mL)
VAD HR (BPM)
0
10
20
30
40
50
0.00
0.05
0.10
0.15
0.20
15
30
45
60
75
90
105

Fig. 5

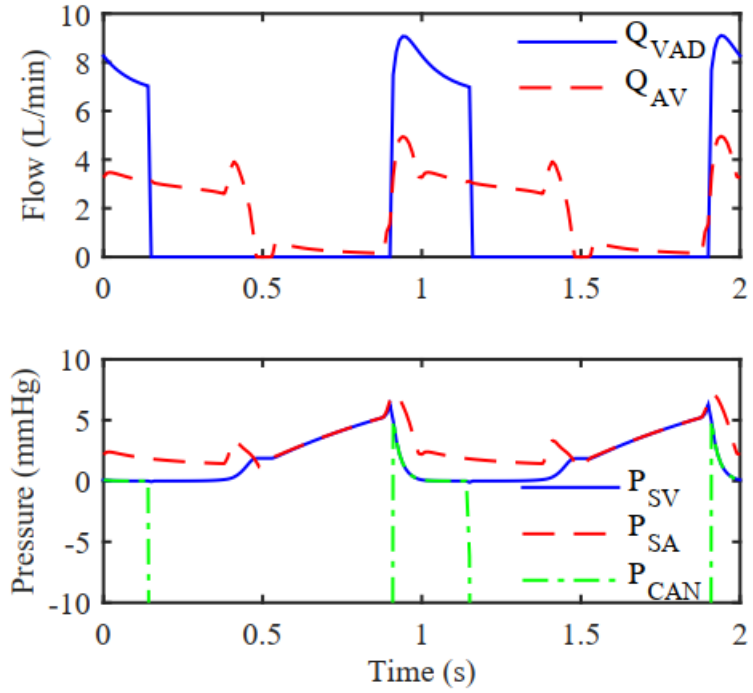
Q_VAD
Q_AV
Flow (L/min)
P_SV
P_SA
P_CAN
Pressure (mmHg)
Time (s)
0
0.5
1
1.5
2
-10
-5
5
10

Supplemental Digital Content

Appendix A

For an LPN, there were two fundamental equations used to calculate the pressure and volumetric flowrate. The general form of the differential equation for pressure was

$$\frac{dP}{dt} = \frac{Q}{C} \tag{A1}$$

and for volumetric flowrate was

$$\frac{dQ}{dt} = \frac{P}{L} \tag{A2}$$

Pressure and flowrate were related to resistance by

$$\Delta P = QR \tag{A3}$$

Atrial and ventricular contraction was represented by an active-passive model. With this model, the pressure can be calculated based on volume and the time in the cardiac period. Two components were present: a passive curve and an active curve for contraction. The passive pressure-volume equation for positive pressures is

$$P_{passive,p} = c\left[e^{d(V-V_0)} - 1\right] \tag{A4}$$

where *c* and *d* are patient specific parameters and V_o is the reference volume. The passive pressure-volume equation for negative pressures is

$$P_{passive,n} = S_n \ln\left(\frac{V}{V_0}\right) \tag{A5}$$

where S_n is a property describing tissue stiffness. The active pressure-volume equation is

$$P_{active} = \frac{V-V_0}{C} \tag{A6}$$

where C is another patient specific parameter.

An activation function describes the period of active contraction for the heart tissue. When contraction occurs, $AA(t)$ takes on a value between zero and one. This is multiplied by P_{active} and adds to the passive pressure. In cases for which atrial pressure was negative, the activation function was set to zero. This was to prevent adding a negative pressure predicted by equation A6 for atrial volumes less than V_0. The general activation function was

$$AA(t) = \begin{cases} \frac{1}{2}\left[1 - \cos\left(2\pi \frac{t - t_1 + t_s}{t_s}\right)\right] & t \le t_1 \\ \frac{1}{2}\left[1 - \cos\left(2\pi \frac{t - t_d - t_1}{t_s}\right)\right] & t_1 + t_d \le t < t_c \\ 0 & else \end{cases} \quad \text{(A7)}$$

where t_1, t_s, t_d, and t_c are the time at end of contraction, total time for systole, total time for diastole, and total time for one cardiac cycle respectively. The equation for calculating the overall pressure is

$$P(V,t) = \begin{cases} P_{active} AA(t) + P_{passive,p} & V \ge 0 \\ P_{passive,n} & V < 0 \end{cases} \quad \text{(A8)}$$

The pressure drop through the systemic-to-pulmonary shunt was calculated with a model by Migliavacca et al. (Migliavacca et al., 2000) and is

$$\Delta P_{SH} = R_{SH} Q_{SH} + K_{SH} Q_{SH}^2 \quad \text{(A9)}$$

where R_{SH} and K_{SH} were patient specific parameters. Similarly, flow through the heart valves was calculated as

$$\frac{dQ_{AV}}{dt} = \begin{cases} 0 & P_{SA} < P_{SV} \; and \; Q_{AV} < 0 \\ \frac{P_{SA} - P_{SV} - K_{AV} Q_{AV}^2}{L_{AV}} & else \end{cases} \quad \text{(A10)}$$

for the atrial-ventricular valve, where K_{AV} is a patient specific parameter, and

$$Q_{AO} = \begin{cases} 0 & P_{SV} < P_{AO} \\ \frac{\sqrt{R_{MYO}^2 + 4K_{AO}(P_{SV} - P_{AO})} - R_{MYO}}{2K_{AO}} & P_{SV} \geq P_{SV} \end{cases} \quad \text{(A11)}$$

for the aortic valve where R_{MYO}, K_{AO} are patient specific parameters.

For the pulsatile flow VAD model to represent a physical system, domain limits on volume were imposed. The volume must remain between zero and the VAD size inclusive. The volume of blood in the VAD was calculated at each iteration as the difference in the time rate of change of volume entering and leaving by

$$\frac{dV_{VAD}}{dt} = \frac{dV_{VAD,IN}}{dt} - \frac{dV_{VAD,OUT}}{dt} \quad \text{(A12)}$$

The time derivative of volume is volumetric flowrate, so a more convenient form is

$$\frac{dV_{VAD}}{dt} = Q_{VAD,IN} - Q_{VAD,OUT} \quad \text{(A13)}$$

Since flow in the VAD cannulas may become turbulent due to high flowrates through a small ID cannula, we use the Darcy-Weisbach equation to model the pressure drop for both laminar and turbulent flow

$$\Delta P = \left(\frac{8 l f_D \rho}{\pi^2 D^5}\right) Q^2 \quad \text{(A14)}$$

where ΔP is the pressure drop, l is the pipe length, f_D is the dimensionless Darcy friction factor, ρ is the fluid density, and D is the pipe diameter. Equation A14 can be directly applied to the VAD cannulas since size dimensions and fluid properties are known. The friction factor is a function of relative roughness, which is the quotient of absolute roughness to pipe diameter, and the Reynolds number. The absolute roughness for Berlin Heart cannulas was assumed a

63 conservative value representative of plastic tubing since no literature was
64 available.

65 For equation A14 to be valid, flow in the cannulas must be incompressible
66 and fully developed. Blood is typically considered incompressible at
67 physiological pressures. Fully developed fluid flow for turbulent Reynolds
68 numbers can occur by 10 diameters of pipe length (Bergman et al., 2011), which
69 occurs for the length majority for cannulas tested in this study.

70 The friction factor, f_D, for the VAD cannulas was calculated using two
71 different equations depending on the flow regime. For laminar flow (Re<2300),
72 the equation was

73 $$f_D = \frac{64}{Re} \quad \text{(A15)}$$

74 and for turbulent flow (Re>2300), the Haaland equation was used

75 $$f_D = \left(-1.8 \log_{10}\left(\left(\frac{\varepsilon}{3.7D}\right)^{1.11} + \frac{6.9}{Re}\right)\right)^{-2} \quad \text{(A16)}$$

76 where ε is the absolute roughness of the cannula material. The units of ε and *D*
77 must match to form a dimensionless ratio.

78 A separate term for the dynamic pressure loss was also included for the
79 inflow and outflow cannulas. This is calculated by

80 $$P = 0.5 k_L \rho V^2 \quad \text{(A17)}$$

81 where k_L is a minor loss factor dependent on geometry and is reported in
82 introductory fluid mechanics textbooks. In practice, it was found that this
83 pressure loss was usually 5 mmHg or less. For example, a k_L of unity with a
84 flowrate of 5 L/min and 12 mm ID cannula would result in a pressure loss of
85 approximately 2.2 mmHg.

The pressure, P_{COMP}, of the pulsatile flow VAD was prescribed explicitly as a function of time by

$$P_{COMP} = \begin{cases} P_{SYS}\left(\sin\left(\frac{t*\pi}{(1-DFR)*t_{VAD}}\right)\right)^{0.1} & systole \\ P_{DIA}\sin\left(\frac{(t-(1-DFR)*t_{VAD})*\pi}{DFR*t_{VAD}}\right) & diastole \end{cases} \quad \text{(A18)}$$

where t_{VAD} is the time of one VAD period and DFR is the diastolic filling ratio (a number between zero and one). An example waveform of equation 1 is shown in Fig. A1.

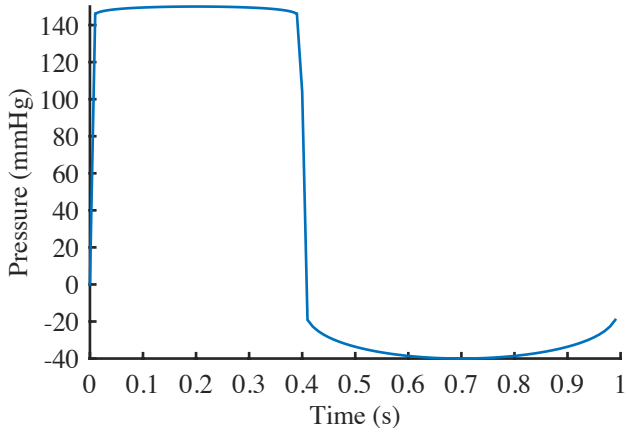

Fig. A1. Equation A18 waveform for settings of P_{SYS} = 150 mmHg, P_{DIA} = -40 mmHg, DFR = 0.60, and t_{VAD} = 1 sec.

We used experimental data from literature for the HeartWare VAD to reconstruct several trendlines in the general form of

$$\Delta P_{VAD} = AQ_{VAD}^2 + BQ_{VAD} + C \quad \text{(A19)}$$

where ΔP_{VAD} is the pressure rise across the VAD, Q_{VAD} is the flowrate through the VAD, and A, B, and C are constants dependent on the RPM of the VAD (Moazami et al., 2013).

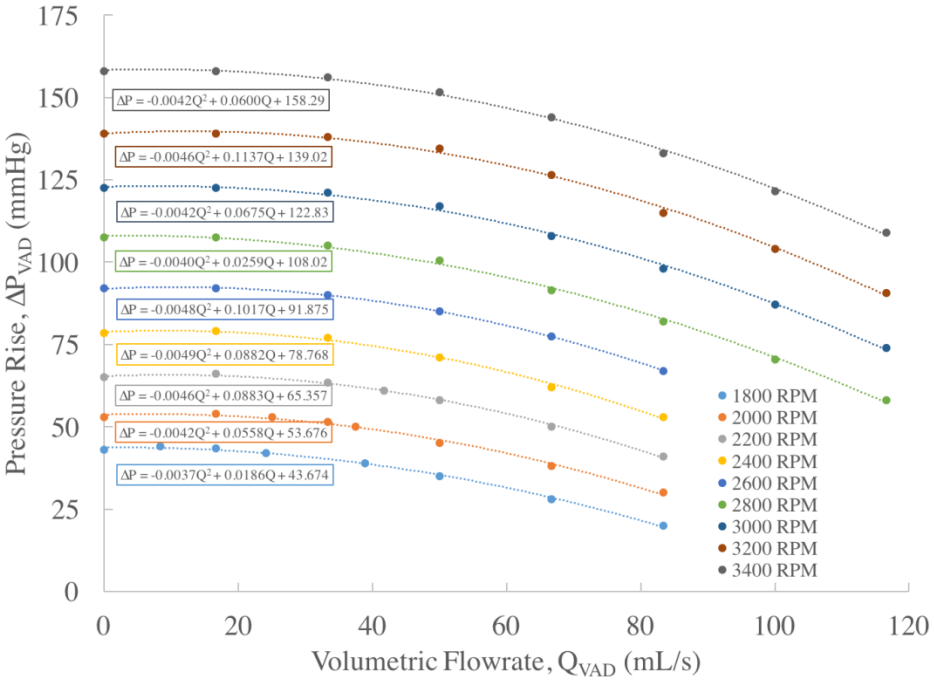

Fig. A2. Reconstructed experimental data with quadratic best fit trendlines for the continuous flow HeartWare VAD

Appendix B

The models from literature for ventricular resistance most suitable for use in our LPN were tested for validity in the pediatric patient circulation under study.

The original concept of suction resistance is traceable to Schima et al. (Schima et al., 1990). Results from that study were later expressed mathematically (Choi, 1998) as

$$R_{SUC} = \begin{cases} 0 & P_{SA} > P_{TH} \\ -3.5P_{SA} + 3.5P_{TH} & P_{SA} \leq P_{TH} \end{cases} \quad \text{(B1)}$$

where R_{SUC} was the suction resistance, P_{SA} was the atrial pressure, and P_{TH} was the threshold pressure for suction to occur. Values of -1 and 0 mmHg have been used for P_{TH} by later studies (Ochsner et al., 2013; Yu and Porter, 2006).

Two previous studies have presented models developed from least squares regression analysis of experimental data from animal experiments. The development of these models was done retrospectively by finding the resistance that best recreated the experimental pressure and flowrate data based on the studied anatomy and physiology.

The first of the two regression models was developed by Yu and Porter (Yu and Porter, 2006) and was

$$R_{SUC} = k + \sum_{i=1,2,3,5} a_i P_{CAN}^i + \sum_{i=1}^{2} b_i P_{SV}^i + c \left| \frac{d}{dt} P_{SV} \right| \quad \text{(B2)}$$

where k is the constant resistance of the VAD cannula itself, P_{CAN} is the pressure in the inflow cannula, P_{SV} is the ventricular pressure, and a, b, and c are constants determined from the regression analysis. Though not explicitly stated by the authors, R_{SUC} was assumed zero for any negative values since a negative resistance has no physical meaning.

130 The second of the regression models was developed by Lim et al. (Lim et
131 al., 2010) and was
132 $$\frac{dR_{SUC}}{dt} = \frac{-R_{SUC}+R_{SUC,\infty}}{\tau_{R_{SUC}}} \quad \text{(B3)}$$
133 where $\tau_{R_{SUC}}$ was a time constant from the regression analysis. $R_{SUC,\infty}$ was
134 modeled by
135 $$R_{SUC,\infty} = \begin{cases} k_{s1}\left(e^{k_{s2}(V_{SV}-V_{TH})}\right) & V_{SV} < V_{TH} \\ 0 & V_{SV} \geq V_{TH} \end{cases} \quad \text{(B4)}$$
136 where k_{s1} and k_{s2} were constants determined from the regression analysis and
137 V_{TH} was the threshold volume for suction to occur. We assumed a zero initial
138 condition for R_{SUC}. The threshold volume originally used by Lim et al. was
139 arbitrarily chosen as the volume at which the left ventricular pressure was equal
140 to 5 mmHg. For consistency with the other suction models tested, we instead
141 chose the ventricular reference volume (for which P_{SV}=0 mmHg) as the threshold
142 volume.
143 Simulations with these models were done for each patient using the 50 mL
144 Berlin Heart at 75 BPM and the HeartWare VAD at 3400 RPM since these
145 settings would have the greatest tendency for ventricular suction to occur (Table
146 B1).
147 Each suction model produced similar results for pulsatile flow, but results
148 varied for continuous flow. For the continuous flow case, the models of Schima
149 and Lim predicted mean pressure drops of approximately 50 mmHg at ventricular
150 pressures close to -1 mmHg. This rapid suction response was unrealistic and
151 these two models were not considered any further. Conversely, the model by Yu

and Porter predicted a pressure drop of only 3.14 mmHg for a ventricular pressure of -7.67 mmHg. This slow suction response was also unrealistic and this model was abandoned as well. It was also expected that complete flow obstruction due to ventricular collapse could occur for the HeartWare VAD by 3400 RPM. This was another reason for dismissing these three models. As a caveat, these models were derived at least in part from animal experiments. Therefore, they may be fairly accurate for circulations more similar to those of the original tests, but they did not appear well suited for pediatric human circulations.

We therefore propose a new model to describe the ventricular suction resistance, R_{SUC}, at negative ventricular pressures. To make the model valid for any BSA, an allometric scaling law between R_{SUC} and anatomical parameters was desired. We define a parameter called the skweeesh factor, Δ, which is expressed as

$$\Delta = D_{SV} + h_{SV} - l_h \quad \text{(B5)}$$

where D_{SV} is the ventricular diameter, h_{SV} is the ventricular wall thickness, and l_h is the cannula head length. If the skweeesh factor equals zero, then the cannula head length equals the ventricular diameter and thickness. In such a situation, the suction resistance would be infinite since no flow can enter the cannula. Therefore, a general relation is established

$$R_{SUC} \propto \frac{1}{\Delta} \quad \text{(B6)}$$

The scale factor of Δ with BSA was obtained by using equation B6 for several BSA values with corresponding ventricular diameter and thickness (Dawson,

2014) and cannula specifications from Berlin Heart. Δ scaled with $BSA^{0.3492}$, and so R_{SUC} scaled with $BSA^{-0.3492}$.

The experimental data during suction events from several studies (Lim et al., 2010; Salamonsen et al., 2015; Schima et al., 1990) was normalized by BSA to recast ventricular suction resistance independent of body size (Fig. B1). A trendline equation (R^2=0.72) was created by doing a best fit for a power model. This model was expressed as

$$R_{SUC} = \begin{cases} 0 & P_{SV} > P_{TH} \\ 0.2623(0.9787^{P_{CAN}} - 1)BSA^{-0.3492} & P_{SV} \leq P_{TH} \end{cases} \quad \text{(B7)}$$

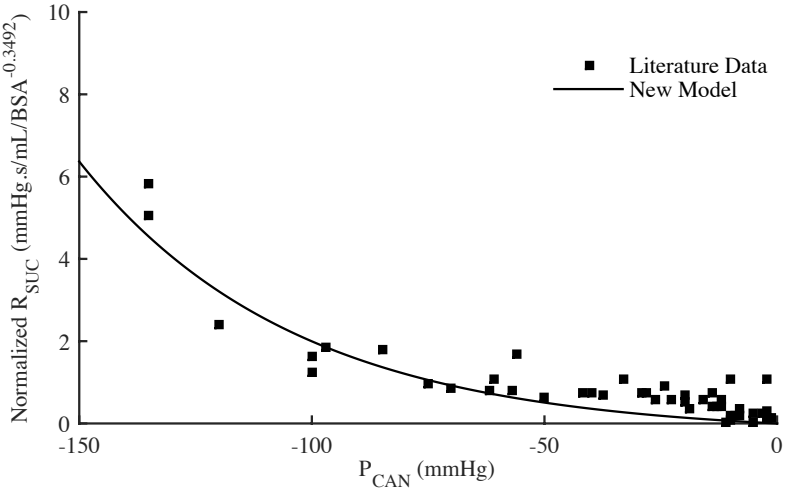

Fig. B1. Experimental suction resistance (R_{SUC}) data obtained from prior studies and normalized by body surface area (BSA).

Additionally, we developed a method to dynamically calculate the threshold pressure for VAD flow to resume. This was derived from a force equilibrium between the negative force caused by cannula suction and the

positive force generated by ventricular pressure. In other words, once a complete flow obstruction occurred, a sufficient positive pressure must build up in the ventricle to "pop off" the inflow cannula from the ventricular wall. The force balance starts with

$$F_{SV} = F_{CAN} \tag{B8}$$

which can be expressed in terms of pressure by

$$P_{TH}A_{SV} = P_{CAN}A_{CAN} \tag{B9}$$

and then ventricular surface area and cannula inner area by

$$P_{TH}(4\pi r_{SV}^2) = P_{CAN}\left(\frac{\pi}{4}D_{CAN}^2\right) \tag{B10}$$

The ventricular radius can be related to BSA by using clinical data (Troy et al., 1972) to obtain

$$r_{SV} = \left(22.4035\,\frac{mm}{m}\right)\sqrt{BSA} \tag{B11}$$

Substituting this expression into the force balance simplifies to

$$P_{TH} = \frac{[P_{CAN}(D_{CAN}^2)]}{[(8031BSA)]} \tag{B12}$$

where D_{CAN} is in mm. Values for the threshold pressure after a complete flow obstruction event typically range from 1-7 mmHg. For reference, a cannula pressure of -100 mmHg, cannula diameter of 12 mm, and BSA of 0.30 m^2 produces a ventricular pressure threshold of 6.0 mmHg.

Using the same suction model testing process, the new model was compared to existing models with respect to its ability to produce realistic physiology for the patients in this study. The new model proposed in this study is named "Proposed" and produced realistic results for both test cases (Table B1).

Although the mean value for R_{SUC} is 43.6 mmHg.s/mL for P_{SV} of 0.45 mmHg, this is because three patients experienced complete flow obstruction. In these cases, R_{SUC} was set arbitrarily to 100 mmHg.s/mL for numerical stability and VAD flow was set to zero until P_{SV} reached P_{TH}. This new model requires further validation from experimentation in future work. Obtaining clinical data in human circulations is difficult since ventricular suction is undesirable in the clinical setting, but this remains an important task to improve accuracy of computational simulation of VAD treatment.

Appendix C

Table C1. Patient specific clinical measurements. Values are expressed as mean for last cardiac period. Q_{UB}, upper body flow; Q_{LB}, lower body flow; Q_{LPV}, left pulmonary vein flow; Q_{RPV}, right pulmonary vein flow; CO, cardiac output; P_{SA}, atrial pressure; P_{AO}, aortic pressure; P_{PA}, pulmonary artery pressure; Q_P/Q_S, ratio of pulmonary to systemic flow.

Patient	A	B	C	D	E	F
Q_{UB} (mL/s)	5.6	10.0	11.2	11.0	8.0	8.3
Q_{LB} (mL/s)	5.7	5.0	5.7	4.0	3.0	6.0
Q_{LPV} (mL/s)	4.5	4.0	2.7	6.5	9.0	8.1
Q_{RPV} (mL/s)	5.2	8.0	4.8	5.5	11.0	8.5
CO (mL/s)	21.0	27.0	24.4	27.0	31.0	29.8
P_{SA} (mmHg)	6.0	7.0	5.0	5.4	4.0	6.0
P_{AO} (mmHg)	52.0	53.0	43.0	53.0	72.0	51.0
P_{PA} (mmHg)	12.0	15.5	13.0	12.7	13.5	11.0
Q_P/Q_S	0.9	0.8	0.4	0.8	1.8	1.1

Table C2. Absolute percent differences between clinical measurements and pre-HF LPN results for each patient. Q_{UB}, upper body flow; Q_{LB}, lower body flow; Q_{LPV}, left pulmonary vein flow; Q_{RPV}, right pulmonary vein flow; CO, cardiac output; P_{SA}, atrial pressure; P_{AO}, aortic pressure; P_{PA}, pulmonary artery pressure; Q_P/Q_S, ratio of pulmonary to systemic flow.

Patient	A	B	C	D	E	F
Q_{UB}	2.3	7.2	4.1	1.3	0.7	4.7
Q_{LB}	1.2	1.4	2.6	2.0	1.0	1.5
Q_{LPV}	4.9	19.8	1.5	2.0	4.8	1.4
Q_{RPV}	8.8	17.3	1.7	4.9	0.2	12.5
CO	1.9	4.4	2.9	1.5	0.5	2.0
P_{SA}	12.0	0.1	30.6	18.5	4.8	6.0
P_{AO}	0.3	2.2	1.9	0.2	0.3	0.2
P_{PA}	2.5	2.1	11.6	9.8	1.7	2.8
Q_P/Q_S	3.5	3.8	2.3	5.0	8.3	7.3

Appendix D

Table D1. Patient specific data for zero ventricular contractility and no VAD support. Values are expressed as mean for last cardiac period. CO, cardiac output; V_{SA}, atrial volume; V_{SV}, ventricular volume; P_{SA}, atrial pressure; P_{SV}, ventricular pressure; P_{AO}, aortic pressure; P_{PA}, pulmonary artery pressure; Q_P/Q_S, ratio of pulmonary to systemic flow.

Patient	A	B	C	D	E	F
CO (L/min)	0.20	0.12	0.04	0.21	0.45	0.16
V_{SA} (mL)	10.11	20.17	11.13	22.84	37.61	21.99
V_{SV} (mL)	37.29	41.01	22.82	48.71	49.59	34.15
P_{SA} (mmHg)	9.77	13.55	15.52	12.31	6.71	10.27
P_{SV} (mmHg)	13.83	15.40	16.29	15.95	15.45	12.08
P_{AO} (mmHg)	13.68	15.30	16.26	15.78	15.14	11.95
P_{PA} (mmHg)	11.26	14.54	15.96	13.8	9.66	10.93
Q_P/Q_S	2.53	2.63	1.27	2.12	4.39	3.91

Table D2. Optimal patient specific outcomes for pulsatile flow (higher of either clinical or modified settings) and continuous flow VADs. Values are expressed as mean for last cardiac period. Patients with V_{MAX} equal to 25 mL had optimal results with 25 mL size Berlin Heart. The settings used to obtain these data are reported in Table E1. CO, cardiac output; V_{SA}, atrial volume; V_{SV}, ventricular volume; P_{SA}, atrial pressure; P_{SV}, ventricular pressure; P_{AO}, aortic pressure; P_{PA}, pulmonary artery pressure; Q_P/Q_S, ratio of pulmonary to systemic flow; R_{SUC}, suction resistance; V_{MIN}, minimum VAD volume; V_{MAX}, maximum VAD volume.

Pulsatile Flow						
Patient	A	B	C	D	E	F
CO (L/min)	1.94	2.37	2.14	2.26	2.21	2.86
V_{SA} (mL)	4.05	9.66	4.33	10.72	25.28	12.59
V_{SV} (mL)	4.29	4.00	6.45	3.95	8.84	7.02
P_{SA} (mmHg)	1.36	1.74	1.06	1.99	2.61	2.32
P_{SV} (mmHg)	0.09	0.10	0.00	0.06	0.52	0.02
P_{AO} (mmHg)	80.83	82.03	60.67	76.74	89.39	87.25
P_{PA} (mmHg)	9.68	12.56	11.40	11.59	13.34	9.08
Q_P/Q_S	0.73	0.61	0.37	0.68	1.61	0.80
R_{SUC} (mmHg.s/mL)	0.10	0.16	0.06	0.16	0.05	0.16
V_{MIN} (mL)	0.00	0.00	0.00	0.00	0.00	0.00
V_{MAX} (mL)	24.76	39.92	25.00	43.70	25.00	48.14
Continuous Flow						
Patient	A	B	C	D	E	F
CO (L/min)	3.11	3.36	3.35	3.50	3.31	4.08
V_{SA} (mL)	0.85	1.10	0.81	1.15	15.14	6.17
V_{SV} (mL)	1.55	1.81	1.47	1.90	3.05	4.10
P_{SA} (mmHg)	-4.68	-1.34	-6.06	-1.48	0.20	0.69
P_{SV} (mmHg)	-6.86	-4.38	-8.25	-4.50	-1.93	-3.58
P_{AO} (mmHg)	133.80	118.60	92.50	117.40	143.01	128.45
P_{PA} (mmHg)	6.90	12.52	8.06	11.45	15.48	9.51
Q_P/Q_S	0.57	0.53	0.31	0.53	1.33	0.69
R_{SUC} (mmHg.s/mL)	0.14	0.10	0.20	0.11	0.03	0.12

Appendix E

We investigated several pulsatile flow VAD settings different from current clinical implementation with the goal of optimizing CO. Investigations were done with the 50 mL Berlin Heart only since mean CO was as much as 37.3% below expected (compared to 0% and 9.7% for the 10 and 25 mL sizes). Since incomplete filling was the limiting factor to CO, adjustments were made to peak VAD pressures and DFR, which are also adjustable in clinical practice. Although flow resistance could be reduced with a larger ID cannula, we chose not model such cases since surgical limitations of the pediatric ventricle would not accommodate cannula ID larger than the 12 mm already modeled. These modifications and combinations of VAD settings were simulated for all patients. Results at 60 BPM produced the highest cardiac index (CI) in all cases while remaining within the limits of the air compressor.

None of the modifications to pulsatile flow VAD settings (Table E1) produced statistically significant differences from clinical implementation simulations (case 1) with respect to CI, and the best result (case 6) produced only a 2.4% increase in CI. When combining the P_{DIA} = -100 mmHg and DFR = 65% settings (case 4), filling improved enough to result in nonzero V_{MIN}, which signaled incomplete ejection, thus we further increased P_{SYS} to improve ejection (case 5). Next, we increased DFR to 80% to further increase time for filling, which produced another 1.0% increase to CI (case 6). Statistically significant increases in R_{SUC} did occur in most cases since improved filling increased the VAD's demand for blood from the ventricle.

Table E1. Modifications to VAD settings for 50 mL Berlin Heart to improve filling. Values are expressed as cohort mean (standard deviation). * denotes statistical significance for $p<0.05$. CI, cardiac index; R_{SUC}, suction resistance; P_{DIA}, peak filling pressure; P_{SYS}, peak ejection pressure; P_{AO}, aortic pressure DFR, diastolic filling ratio.

Case	VAD Setting Change	Rationale	CI ($L/min/m^2$)	R_{SUC} (mmHg.s/mL)	CI *p*-Value	R_{SUC} *p*-Value
1	Control		7.63 (1.72)	0.06 (0.01)		
2	P_{DIA} = -100 mmHg	Larger pressure gradient for filling	7.63 (1.72)	0.12 (0.01)	1.0000	$1.940.10^{-5}$*
3	DFR = 65%	Increased time for filling	7.64 (1.74)	0.07 (0.01)	0.9854	0.1902
4	P_{DIA} = -100 mmHg DFR = 65%	Combine cases 2 and 3	7.65 (1.74)	0.13 (0.01)	0.9707	$3.706.10^{-6}$*
5	$P_{SYS} = P_{AO}$+200 mmHg P_{DIA} = -100 mmHg DFR = 65%	Incomplete ejection occurred in case 4, thus increased peak ejection pressure	7.73 (1.77)	0.13 (0.01)	0.8777	$8.992.10^{-7}$*
6	$P_{SYS} = P_{AO}$+200 mmHg P_{DIA} = -100 mmHg DFR = 80%	Further increased time for filling	7.81 (1.78)	0.16 (0.01)	0.7729	$6.018.10^{-9}$*

Reference

Bergman, T.L., Lavine, A.S., Incropera, F.P., DeWitt, D.P., 2011. Introduction to Heat Transfer, 6th ed. John Wiley & Sons, Inc, Jefferson City, MO.

Dawson, T., 2014. Allometric relations and scaling laws for the cardiovascular system of mammals. Systems 2, 168–185. doi:10.3390/systems2020168

Migliavacca, F., Dubini, G., Pennati, G., Pietrabissa, R., Fumero, R., Hsia, T.Y., de Leval, M.R., 2000. Computational model of the fluid dynamics in

294 systemic-to-pulmonary shunts. J. Biomech. 33, 549–57. doi:10.1016/s0021-
295 9290(99)00219-5

296 Ochsner, G., Amacher, R., Daners, M.S., 2013. Emulation of ventricular suction
297 in a hybrid mock circulation. 2013 Eur. Control Conf. 3108–3112.

298 Troy, B.L., Pombo, J., Rackley, C.E., 1972. Measurement of left ventricular wall
299 thickness and mass by echocardiography. Circulation 45, 602–611.
300 doi:10.1161/01.CIR.45.3.602